Available online at www.sciencedirect.com
ScienceDirect
International Journal of Heat and Mass Transfer 51 (2008) 5400–5414
International Journal of HEAT and MASS TRANSFER
www.elsevier.com/locate/ijhmt

High heat flux flow boiling in silicon multi-microchannels – Part I: Heat transfer characteristics of refrigerant R236fa

Bruno Agostini [a], John Richard Thome [a,*], Matteo Fabbri [b], Bruno Michel [b], Daniele Calmi [b], Urs Kloter [b]

[a] Heat and Mass Transfer Laboratory (LTCM), École Polytechnique Fédérale de Lausanne (EPFL), CH-1015 Lausanne, Switzerland
[b] IBM Zürich Research Laboratory, Säumerstrasse 4/Postfach, CH-8803 Rüschlikon, Switzerland

Received 14 April 2007
Available online 29 May 2008

Abstract

This article is the first in a three part study on flow boiling of refrigerants R236fa and R245fa in a silicon multi-microchannel heat sink. The heat sink was composed of 67 parallel channels, which are 223 μm wide, 680 μm high and 20 mm long with 80 μm thick fins separating the channels. The base heat flux was varied from 3.6 to 221 W/cm^2, the mass velocity from 281 to 1501 kg/m^2 s and the exit vapour quality from 2% to 75%. The working pressure and saturation temperature were set nominally at 273 kPa and 25 °C, respectively. The present database includes 1217 local heat transfer coefficient measurements, for which three different heat transfer trends were identified, but in most cases the heat transfer coefficient increased with heat flux and was almost independent of vapour quality and mass velocity. Importantly, it was found for apparently the first time that the heat transfer coefficient as a function of vapour quality reaches a maximum at very high heat fluxes and then decreases with further increase of heat flux.

Keywords: Flow boiling; Microchannel; High heat flux; Chip cooling; Refrigerant

1. Introduction

Heat transfer in microchannels is gaining significant attention in the heat transfer community, mainly because the micro-electronics industry is faced with increasingly high heat fluxes to dissipate. It is expected that in a few years chips dissipating heat fluxes as high as 300 W/cm^2 will have to be cooled while still operating at 85 °C maximum. Numerous studies are already available on liquid-phase heat transfer in microchannels. Recent studies [1–5] showed that a conventional analysis approach can be employed in predicting single-phase heat transfer behaviour in microchannels provided however that surface roughness and entrance effects, axial conduction and viscous heating are taken into account. While water cooling in multi-microchannels seems to be the preferred solution for micro-electronics cooling for the short term, it has the disadvantages of large temperature gradients along the chip, a high freezing point temperature and the dangers of using water close to electrical connections, problems that flow boiling of a refrigerant in multi-microchannels does not have. A state-of-the-art analysis of high heat flux cooling technologies by Agostini et al. [6] showed that flow boiling in microchannels is a very promising approach for high heat flux removal for the medium to long term.

Compared to single-phase flow, however, fewer experimental data are available for flow boiling in microchannels. Furthermore, Agostini et al. [7] demonstrated that out of 13 of the most recent studies on flow boiling in microchannels, 8 exhibited totally different and sometimes contradictory heat transfer trends. Actually many of the studies presenting flow boiling heat transfer coefficients did not validate their test setups beforehand with single-phase flow experiments, meaning there is no way to assess the validity

* Corresponding author. Tel.: +41 21 693 5981; fax: +41 21 693 5960.
E-mail address: john.thome@epfl.ch (J.R. Thome).
URL: http://ltcm.epfl.ch (J.R. Thome).

0017-9310/$ - see front matter © 2008 Elsevier Ltd. All rights reserved.
doi:10.1016/j.ijheatmasstransfer.2008.03.006

Nomenclature

A	flow area (m^2)
A_1, A_2	constants in Fig. 13 (W/m^2 K)
$B = N \cdot W + (N-1) \cdot 2t$	multi-channel footprint width (m)
$Bo = q/(G \cdot h_{lv})$	boiling number
c_p	specific heat capacity (J/kg K)
$D_h = 2W \cdot H/(W+H)$	hydraulic diameter (m)
e	distance from RTDs to channels base (m)
$4f$	friction factor
G	mass velocity (kg/m^2 s)
h_{lv}	latent heat of vapourisation (J/kg)
H	channel height (m)
I	current (A)
k	thermal conductivity (W/m K)
L	channel length (m)
m	fin parameter
N	number of channels
$Nu = \alpha \cdot D_h/\lambda$	Prandtl number
$Pr = \mu \cdot c_p/\lambda$	Prandtl number
p	pressure (Pa)
q	heat flux (W/m^2)
$Re = (G \cdot D_h)/\mu_l$	Reynolds number
t	fin half width (m)
T	temperature (K)
U	voltage (V)
v	specific volume (m^3/kg)
W	channel width (m)
x	vapour quality
z	z coordinate (m)
z_+	dimensionless z coordinate (m)

Greek symbols

α	heat transfer coefficient (W/m^2 K)
δ	roughness (μm)
Δp	pressure loss (Pa)
$\Delta T_{sub} = T_{fl,i} - T_{sat}$	inlet sub-cooling (K)
ϵ	fin efficiency
μ	dynamic viscosity (Pa s)
ρ	mass density (kg/m^3)
σ	surface tension (N/m)
ξ	singular pressure loss coefficient

Subscripts

a	accelerational
b	base
f	friction
fin	fin
fl	fluid
hom	homogeneous
in	inlet
l	liquid
m	mean
meas	measured
out	outlet
sat	saturation
Si	silicon
TP	two-phase
v	vapour
w	wall
z	local along z

of these various heat transfer trends. However, of these eight different trends, the following two were represented in 11 out of 13 studies:

- at low to moderate vapour quality (typically for $x < 0.5$), the heat transfer coefficient increased with heat flux and decreased slightly or was constant with increasing vapour quality;
- at higher vapour quality, the heat transfer coefficient decreased sharply with increasing vapour quality and did not depend on the heat flux or mass velocity.

Interestingly, experimental studies presenting single-phase validation of the flow boiling measurements, like Agostini and Bontemps [8] and Shiferaw et al. [9] typically show these two dominant trends.

A review of experiments and theory on boiling in microchannels by Thome [10] concluded that macroscale models are not realistic for predicting flow boiling coefficients in microchannels as the controlling mechanism is not nucleate boiling nor turbulent two-phase convection but is transient thin film evaporation. For microchannels, Thome et al. [11] and Dupont et al. [12] proposed a three-zone model based on transient thin film evaporation that is able to predict the two heat transfer trends previously described. Concerning pressure drop during flow boiling in microchannels, a recent literature study by Ribatski et al. [13] demonstrated that the homogeneous model and the Müller-Steinhagen and Heck [14] correlation were the best two methods for predicting two-phase pressure drops in microchannels. Their comparison included pressure drop data from nine independent laboratories that covered both diabatic and adiabatic results for eight fluids, mass velocities from 23 to 6000 kg/m^2 s and vapour qualities up to 1. Thus, it seems that for pressure drop the situation is actually simpler in microchannels than in macrochannels and that basic models like the homogeneous model can be tentatively used. On the other hand, Revellin et al. [15] have shown that these methods only work when the two-phase homogeneous Reynolds number (calculated using McAdams [16] viscosity expression) is larger than 8000 and that no method works below these values. Interestingly, they found a Moody-like diagram for two-phase flows in microchannels for Reynolds numbers from 1000 to 30,000.

Recently, Schneider et al. [17] used small orifices to initiate nucleation at the inlet of a multi-microchannels array with 227 μm hydraulic diameter channels and refrigerant R123, with heat fluxes up to 213 W/cm^2, and found that the heat transfer coefficient was enhanced by this method by up to 84%. The same method was used in the present study.

Wang et al. [18] have investigated the unstable and stable flow boiling of water in parallel microchannels and in a single channel. The hydraulic diameter and length of their channel was 186 μm and 30 mm, respectively, close to the geometry of the present study. According their study, stable flow conditions occurred for $q/G < 0.96$ kJ/kg, which corresponds to the present experimental conditions and indeed no instabilities were observed. Of course results obtained with water are probably not directly usable for refrigerant, but the trend that low heat flux and high mass velocity favours stable flow should hold.

Practical cooling applications will use parallel multi-microchannels and not single channels so that other issues like flow instabilities, back flow, possibly early or delayed critical heat flux, have to be addressed as pointed out by Bergles and Kandlikar [19]. As a consequence, although flow boiling in single microchannels helps in understanding the fundamental processes, the experimental study of flow boiling in microchannel heat sinks is necessary, which is the motivation of the present study. To the best of our knowledge, the only experimental study available for refrigerant flow boiling at high heat fluxes in microchannel heat sinks was recently done by Lee and Mudawar [20] in 2005 with refrigerant R134a flowing in 0.231 mm wide and 0.713 mm high parallel copper microchannels, with base heat fluxes as high as 93.8 W/cm^2. Their heat transfer coefficients increased with heat flux and decreased with vapour quality, which seems to be the typical trend in microchannels as noted earlier. Their test section on the other hand had only one thermocouple to measure the multi-channel base temperature, which did not allow them to investigate local effects along the channels.

Based on the above considerations, it was decided for the present study to perform local heat transfer coefficient measurements at five locations along a silicon multi-microchannel heat sink with refrigerant R236fa at a nominal saturation temperature of 25 °C and saturation pressure of 273 kPa, with liquid flow at the inlet, heat fluxes up to 221 W/cm^2 (limit of the test facility) and mass velocities between 300 and 1600 kg/m^2 s. R236fa was chosen for its low working pressure and its various other advantages (low freezing point, saturation pressure above ambient at ambient temperature and it is inflammable). These are apparently the first microchannel boiling results to be obtained with this refrigerant. In order to optimize a multi-microchannel cooling element with flow boiling, the influence of every parameter of importance on the heat transfer coefficient must be accurately known. Thus, the main purpose of the present study was to investigate the characteristics of flow boiling of this refrigerant in parallel multi-microchannels as it seems to be a good candidate for these applications.

This study is composed of three parts. Part I presents the test facility, data reduction method, the local heat transfer coefficients measured for refrigerant R236fa. In part II, the local heat transfer coefficients measured for R245fa, another low pressure refrigerant, are presented and then compared with the refrigerant R236fa data and to several microscale boiling heat transfer prediction methods. Finally, in part III, critical heat flux results and pressure drop data will be presented and analysed.

2. Experimental setup

The experimental setup is shown in Fig. 1. It was built at the IBM Zürich Research Laboratory. It is composed of a test section, a condenser with a cooling bath, a liquid pump (Fluidotech model MGBR2), a pre-heater with a heating bath, a 7 μm filter and a Coriolis mass flowmeter (Krohne Optimass 3050F). A reservoir is used to store the refrigerant and to accurately control the working pressure. This reservoir is connected to the loop with a T junction between the filter and the flowmeter. A helically coiled copper tube runs inside this reservoir and is connected to a controlled temperature bath so that the refrigerant can be condensed or evaporated to reach the desired pressure inside the flow loop. Sight glasses and valves are situated at various locations in the loop.

This test loop is also instrumented with two K type thermocouples to measure the fluid inlet and outlet temperatures, an absolute pressure transducer (Omega PAA33-V-30, ±1.5 kPa fullscale) to measure the fluid inlet pressure and a differential pressure transducer (Omega PD23-V-1, ±0.5 kPa fullscale) to measure the fluid pressure drop across the entire test section, including the inlet and outlet headers.

The silicon die used as the test section is shown in Fig. 2. It is 1 mm thick and 31 × 31 mm in size. Multi-microchannels have been etched into the upper face with an inductively coupled plasma etching process (dry etching) and are shown highly magnified in Fig. 3 (the magnification is increased in the successive three pictures starting from the top. The second and third pictures represent a close-up on one wall of the channels). There are 67 parallel channels, which are 20 mm long, 223 μm wide and 680 μm high with a fin width of 80 μm. The dimensions of the sections of the channels have been checked with electron microscopy. As shown in Fig. 4, a LEXAN plate (1 mm thick) is glued on the top of the silicon die with a 0.5 mm wide inlet slit and a 1 mm wide outlet slit. The glue is applied at the periphery of the silicon die only so that no glue can overflow into the channels and a force was applied on top during operation. Thus a tiny gap might exist between the LEXAN plate and the silicon die. However, since the flow enters as liquid and the inlet manifold diameter (6 mm) is much bigger than the channel size, the flow distribution is expected to be uniform. No bypass flow could

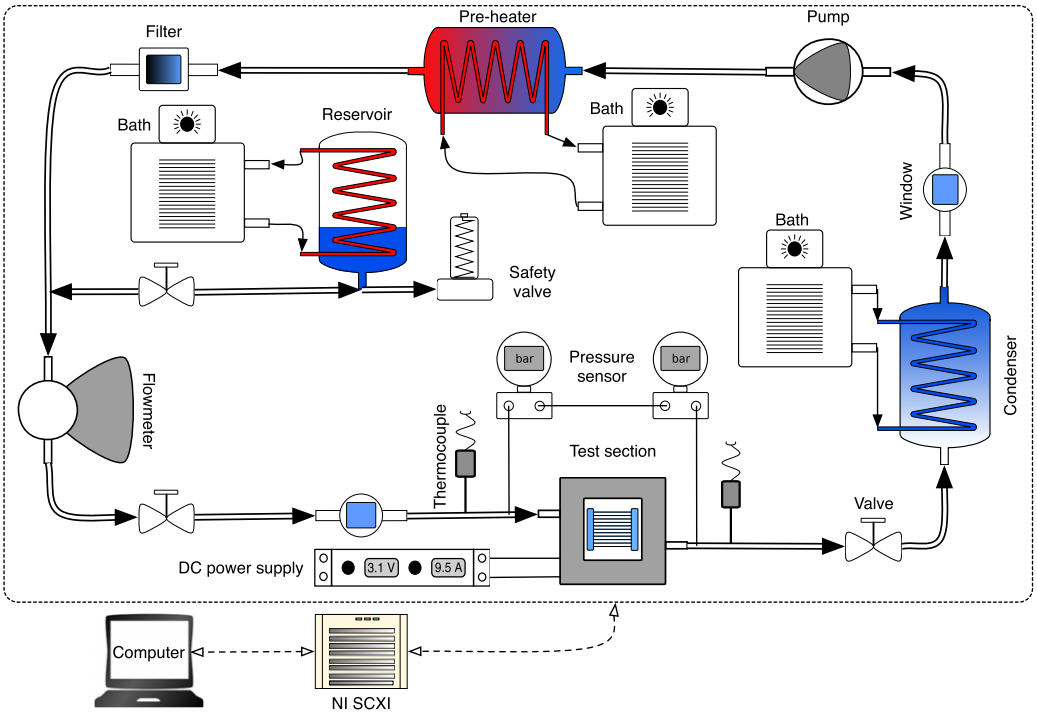

Fig. 1. Flow boiling test loop.

be detected by visual inspection. On the top of this plate, a LEXAN cover with one inlet and one outlet plenum is also added. Overlaying the plate with the slits on the die with the channels creates an orifice (500 × 223 μm) at the inlet of each channel, which are useful to inhibit flow instabilities and backflow as advocated by Bergles and Kandlikar [19]. Note that the inlet singular pressure drop is thought to be primarily due to the abrupt 90° change in flow direction rather than to the flow area reduction.

A serpentine multi-layer resistance heater (10 nm of titanium, 1 μm of gold, 30 nm of nickel and 30 nm of gold) was deposited on the lower face of the die with a lithography process. As shown in Fig. 2, it is composed of six parallel strips that are 0.5 mm wide each with five 180° turns, thus forming six 3 mm wide arms. The refrigerant flows in the microchannels from left to right across the heater. RTDs with an electrical resistance of 59 Ω (same composition as the heater, 10 μm wide) have been deposited with the same process at five different locations between two successive arms of the heater. The sensitive length of these RTDs is about one-third of the width occupied by the channels and they are perpendicular to the channels so that they measure the base temperature at five locations along the channels, averaged on one-third of the total number of channels and centered on the middle channel. The distance between the RTDs and the bottom of the channels is 320 μm. The total width occupied by the 67 channels is 20 mm. The five RTDs are placed at 3.267, 6.534, 9.801, 13.068 and 16.335 mm from the beginning of the channels.

The two thermocouples and five RTDs were calibrated in a temperature controlled bath with a precision thermometer (Merck AG model 26) between 5 and 70 °C. The electrical resistance of the RTDs was measured with a four points measurement technique and an independent power supply providing a 1 mA current source. The uncertainty on the temperature measurements after calibration was estimated to be ±0.1 K.

The heater was connected to a Agilent 6674A DC power supply providing 60 V and 35 A maximum. The voltage and current were measured by the power supply itself with an accuracy of 0.05% + 90 mV for voltage and 0.1% + 35 mA for current. The test loop is controlled and the data recorded with a SCXI National Instruments acquisition system composed of a SCXI-1102 module with a 2 Hz filter.

The test loop was evacuated with a vacuum pump for 24 h before being filled. Since the operating pressure is above the atmospheric pressure, no contaminant can enter the fluid. The R236fa is shipped in a pressurised bottle and is free of any contaminant, thus degasing is not necessary (the measured saturation temperatures and pressures matched closely those of its vapour pressure curve).

3. Operating conditions

The working pressure was set at 273 kPa and was kept constant within ±10 kPa due to the temperature control inside the reservoir. The corresponding saturation temperature variation is ±0.5 K. Note that the pressure was kept constant at ±2 kPa for 90% of the data, meaning the saturation temperature variation is ±0.1 K. The condenser inlet temperature was set at 5 °C so that the sub-cooling at the

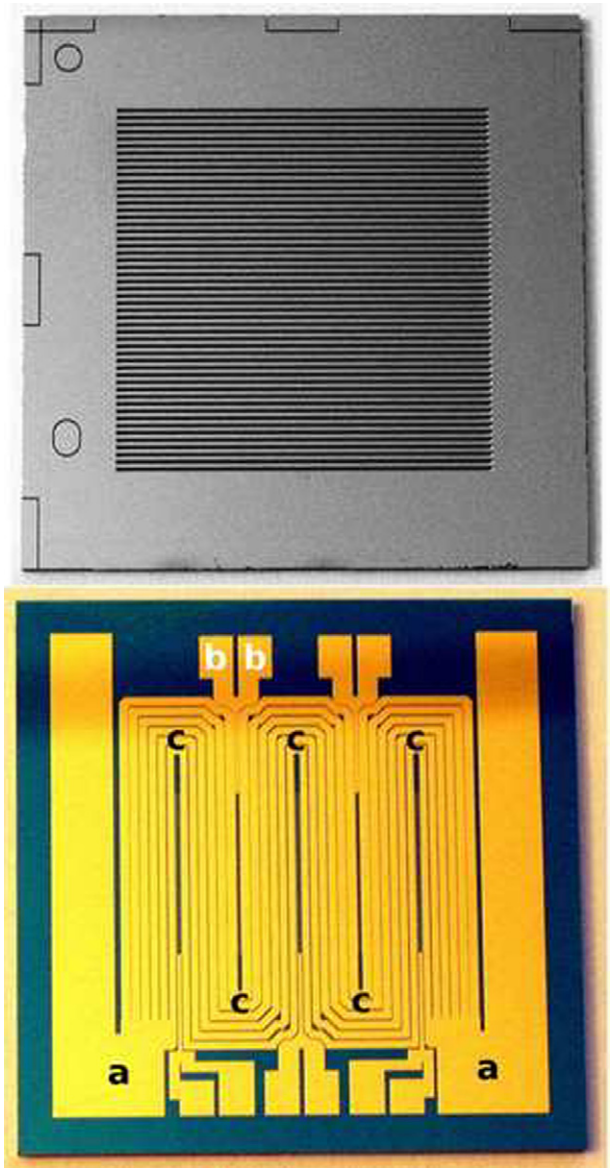

Fig. 2. Silicon test die photographs. Top: multi-microchannel. Bottom: (a) cobra heater, (b) connectors for one RTD, (c) the five RTDs.

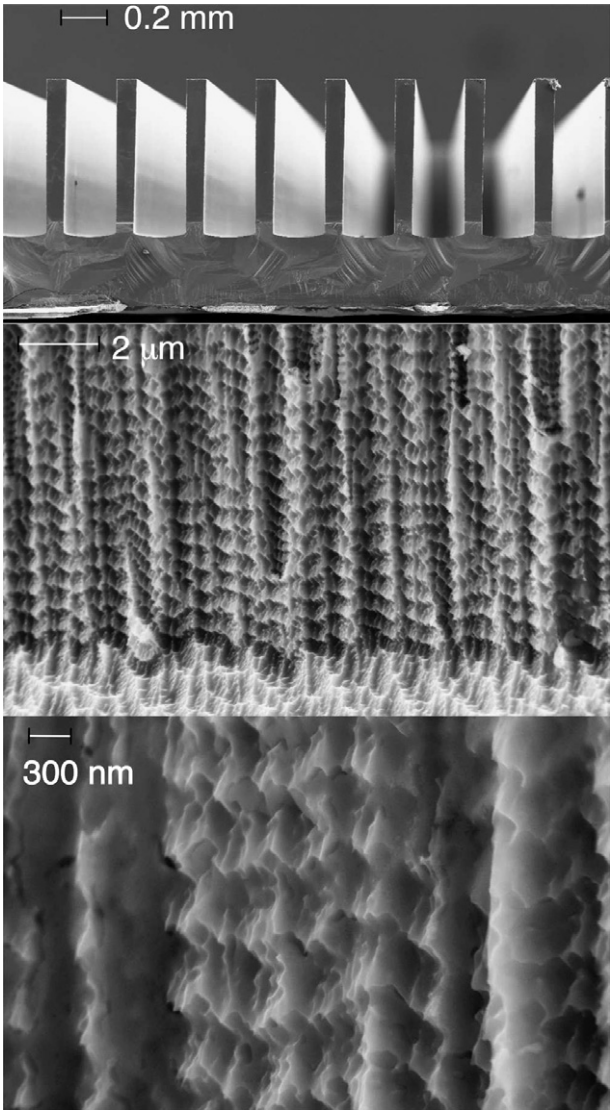

Fig. 3. Scanning electron microscope photograph of the multi-microchannels at three different scales. The middle and bottom figures are close-ups of the fin wall.

inlet of the pump is large enough to avoid cavitation. The pre-heater temperature was set at 25 °C so that the sub-cooling is 0 K (±0.5 K) at the inlet of the test section. (Note that the sub-cooling can take small positive values since a superheat or a pressure drop is necessary to initiate bubble nucleation.) A small amount of flashing at the inlet of the channels was created by the small orifices at the inlet of each channel. Thus, evaporation started without a temperature overshoot that is usually necessary to initiate nucleation in a liquid and the data were more reliable and reproducible. This process is also interesting for the actual application for cooling of a microprocessing chip since it avoids a local temperature overshoot, which would possibly be harmful to the chip. Note that the saturation temperature of the system is calculated using the inlet pressure.

4. Data reduction

First of all, the base heat flux q_b is

$$q_b = \frac{U \cdot I}{L \cdot B} \tag{1}$$

where L is the heated length and B is the heated width.

The two-phase pressure drop is generally high in microchannels so that the saturation temperature can decrease by several degrees along the channels. As a consequence, the pressure at the location of each RTD must be calculated in order to know the local saturation temperature. The measured total pressure drop through the test section during boiling tests includes the pressure drop of the single-phase liquid flow at the inlet, the two-phase flow pressure drop along the channels and the outlet pressure drop. As shown in Fig. 5, the inlet single-phase pressure

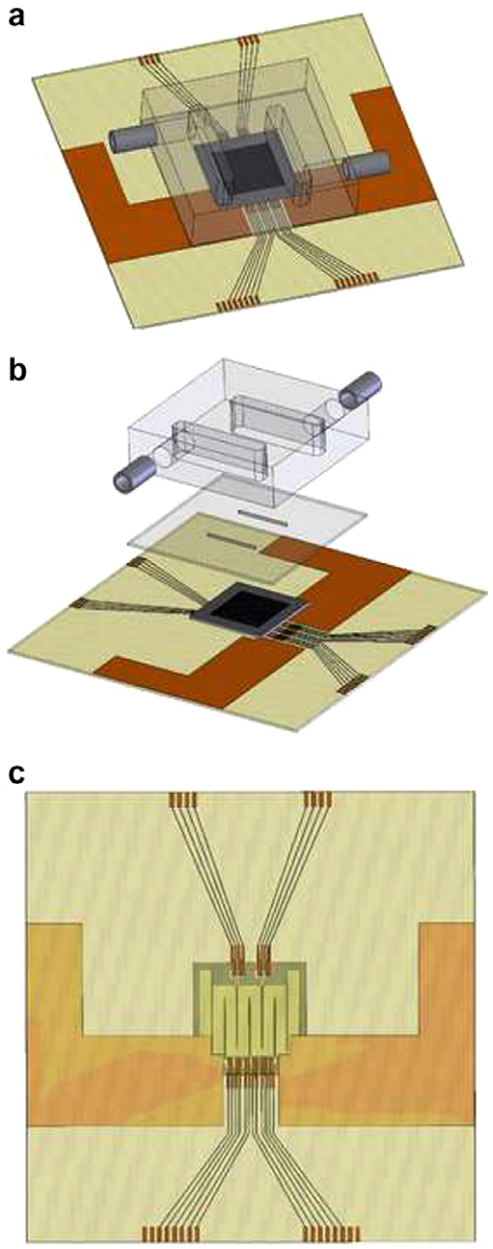

Fig. 4. Test section: (a) assembled view, (b) split view: the manifold block and plate with slits providing flow restriction are visible, (c) back view with RTD connections: the serpentine structure of the heater and the location of RTDs at each fold are visible.

drop can be calculated from a curvefit to the measured pressure drops taken for a sub-cooled liquid flow. As the outlet slit is twice as large as the inlet slit, the outlet pressure drop in the completely sub-cooled tests is approximately one seventh that of the inlet pressure drop (calculated with Idel'cik [21]) and can be neglected. The frictional pressure drop of the sub-cooled liquid along the channels is calculated as

$$\Delta p_{\mathrm{f}} = \frac{G^2}{2\rho_{\mathrm{l}}} \cdot 4f \cdot \frac{L}{D_{\mathrm{h}}} \tag{2}$$

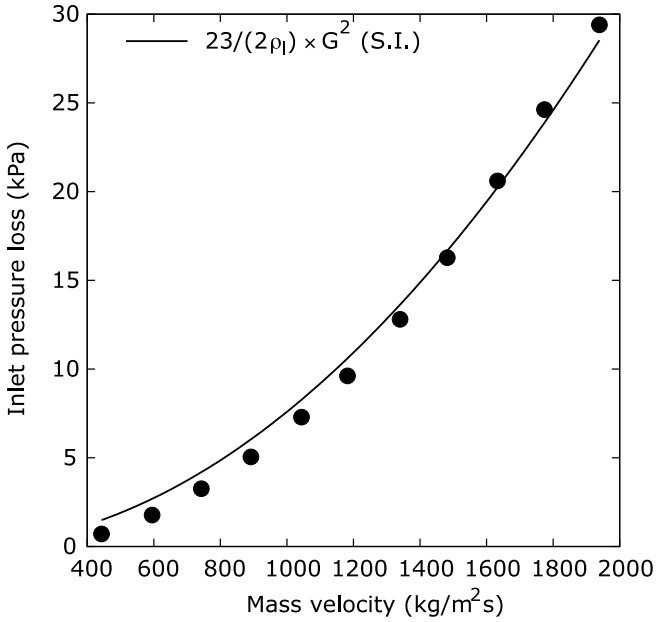

Fig. 5. Singular pressure loss of liquid at inlet versus mass velocity.

where $4f$ is the friction factor for a hydrodynamic developing flow and is calculated with the numerical solution of Shah and London [22] as

$$4f = \left(68.64 + \frac{2.46}{z_+^{0.74}}\right) \cdot \frac{1}{Re} \tag{3}$$

with

$$z_+ = \frac{z}{Re \cdot Pr \cdot D_{\mathrm{h}}}. \tag{4}$$

Finally, the inlet pressure drop is

$$\Delta p_{\mathrm{in}} = \Delta p_{\mathrm{meas}} - \Delta p_{\mathrm{f}} = \frac{G^2}{2\rho_{\mathrm{l}}} \cdot \xi, \tag{5}$$

where ξ is the inlet singular pressure loss coefficient. With the polynomial fit shown in Fig. 5, ξ was found to be equal to 23 for the present inlet configuration.

The two-phase pressure drop along the channels is then calculated as follows. The homogeneous model was used to calculate the pressure drop along the microchannels since Ribatski et al. [13] demonstrated that the homogeneous model was suitable for this purpose. The two-phase frictional pressure drop is thus calculated as

$$-\left(\frac{\mathrm{d}p}{\mathrm{d}z}\right)_{\mathrm{f}} = \frac{G^2}{2\rho_{\mathrm{TP}}} \cdot 4f_{\mathrm{TP}} \cdot \frac{1}{D_{\mathrm{h}}} \tag{6}$$

with

$$\rho_{\mathrm{TP}} = \frac{1}{v_{\mathrm{TP}}} = \frac{1}{x \cdot v_{\mathrm{v}} + (1-x) \cdot v_{\mathrm{l}}} \tag{7}$$

$$Re_{\mathrm{TP}} = \frac{G \cdot D_{\mathrm{h}}}{\mu_{\mathrm{TP}}} \tag{8}$$

$$\mu_{\mathrm{TP}} = (1-x) \cdot \mu_{\mathrm{l}} + x \cdot \mu_{\mathrm{v}} \tag{9}$$

$$4f_{\mathrm{TP}} = 0.316 \cdot Re_{\mathrm{TP}}^{-0.25} \tag{10}$$

where the hydraulic diameter of the channels is 336 μm. μ_{TP} is the two-phase viscosity calculated using the Ciccitti et al. [23] definition. The accelerational pressure drop gradient is

$$-\left(\frac{dp}{dz}\right)_a = G^2 \cdot \frac{dv_{TP}}{dz} = G^2 \cdot \left[(v_v - v_l)\cdot\frac{dx}{dz} + x\cdot\frac{dv_v}{dp}\cdot\left(\frac{dp}{dz}\right)_{hom}\right] \quad (11)$$

The gravitational pressure drop gradient is null in the present case since the flow is horizontal. Thus, the total pressure drop gradient is

$$-\left(\frac{dp}{dz}\right)_{hom} = \frac{G^2\cdot(v_v - v_l)\cdot\frac{dx}{dz} + \frac{G^2}{2\rho_{TP}}\cdot 4f_{TP}\cdot\frac{1}{D_h}}{1 + G^2\cdot x\cdot\frac{dv_v}{dp}} \quad (12)$$

The term dv_v/dp was evaluated with the REFPROP 7.0 software from NIST and is equal to $-2\times10^{-8}\ m^4\ s^2/kg^2$ at the operating saturation temperature. Finally, the local pressure along the channels can be calculated as

$$p(z) = p_{in} - \frac{G^2}{2\rho_l}\cdot\xi - \int_0^z \left(\frac{dp}{dz}\right)_{hom} dz. \quad (13)$$

The homogeneous pressure gradient depends on the vapour quality so that the local vapour quality was calculated using a heat balance over the length dz taking into account the flashing effect along the channels, which is not negligible in microchannels:

$$B\cdot q_b\cdot dz = A\cdot G\cdot[x\cdot c_{p,v}(T_{sat})\cdot dT_{sat} + (1-x)\cdot c_{p,l}(T_{sat})\cdot dT_{sat} + h_{lv}(T_{sat}+dT_{sat})\cdot dx] \quad (14)$$

yielding

$$dx = \frac{(B\cdot q_b\cdot dz)/(A\cdot G) - (x\cdot c_{p,v}(T_{sat}) + (1-x)\cdot c_{p,l}(T_{sat}))\cdot dT_{sat}}{h_{lv}(T_{sat}+dT_{sat})} \quad (15)$$

Accordingly, the vapour quality variation due to the flashing effect at the rectangular inlet orifices was calculated as

$$dx_{in} = \frac{[x\cdot c_{p,v}(T_{fl}(0)) + (1-x)\cdot c_{p,l}(T_{fl}(0))]\cdot dT_{sat}(0)}{h_{lv}(T_{fl}(0)+dT_{sat}(0))} \quad (16)$$

with

$$dT_{sat} = T_{sat}(p_{in} - \xi\cdot G^2/2\rho_l) - T_{fl}(0) \quad (17)$$

$T_{fl}(0)$ being the fluid inlet temperature.

Eqs. (13) and (15) must be solved iteratively starting from the inlet of the channels. Thus, the flow length was divided into 100 increments and the fluid pressure and vapour quality variation is then calculated for each $dz = L/100$.

The fluid saturation temperature is calculated from the vapour pressure curve, knowing the local pressure:

$$T_{fl}(z) = T_{sat}(p(z)) \quad (18)$$

For single-phase liquid flow tests, the local fluid temperature is calculated iteratively along the channels with an energy balance:

$$T_{fl}(z) = T_{fl}(0) + \int_0^z \frac{B\cdot q_b\cdot dz}{A\cdot G\cdot c_{p,l}(z)} \quad (19)$$

The local heat transfer coefficient is calculated by

$$\alpha(z) = \frac{q_w}{T_w(z) - T_{fl}(z)} \quad (20)$$

with T_{fl} being either the saturation temperature given by Eq. (18) for flow boiling tests or the liquid fluid temperature given by Eq. (19) for liquid single-phase tests, respectively. The channel base temperature T_w is calculated from the measured die base temperature T_b assuming one-dimensional heat conduction, since the distance between the base of the chip and the base of the channels is very small ($e = 0.32$ mm):

$$T_w = T_b - \frac{q_b\cdot e}{k_{Si}} \quad (21)$$

The thermal conductivity of silicon depends on temperature with the following relationship from 27 to 127 °C (from Shanks et al. [24] adapted for n-doped silicon):

$$k_{Si} = 0.0018\cdot T^2 - 0.7646\cdot T + 143.25 \quad (22)$$

so that Eq. (21) is solved iteratively by dividing e into 100 increments. This variation in k_{Si} must be taken into account because the thermal conductivity of silicon varies from 124 to 91 W/m K between 27 and 85 °C, which means that an error of about 2 K would occur at 220 W/cm^2 compared to a 5 °C temperature gradient over the thickness of 0.32 mm if the value of k_{Si} at 27 °C was used.

The wall heat flux is calculated with the fin efficiency formula for $(N-1)$ parallel rectangular fins:

$$q_w = q_b\cdot\frac{N\cdot(2t+W) - 2t}{2(N-1)\cdot(H+t)\cdot\epsilon + N\cdot W} \quad (23)$$

with

$$\epsilon = \frac{\tanh(m\cdot(H+t))}{m\cdot(H+t)} \quad (24)$$

$$m = \sqrt{\frac{\alpha\cdot(L+2t)}{k_{Si}\cdot t\cdot L}} \quad (25)$$

assuming that the temperature at the base of the channels is uniform across the channels (i.e., in the direction perpendicular to the flow direction) and that the heat transfer coefficient is uniform along the perimeter of the channels. Eqs. (20) and (23)–(25) are solved together iteratively with a fixed point method since α and ϵ are interdependent. Furthermore, k_{Si} is evaluated at the fin average temperature, which is estimated as

$$\overline{T_{fin}} \approx \frac{T_b + T_{fin}(H)}{2} \quad (26)$$

and

Table 1
Operating conditions and measurement uncertainties

	Value	Error
L (mm)	20	±0.02
B (mm)	20	±0.02
N	67	–
W (μm)	223	±10
H (μm)	680	±10
e (μm)	320	±10
$2t$ (μm)	80	±10
D_h (μm)	336	±27
R_w (nm)	160	±50
G (kg/m^2 s)	281–1501	±3%
q_b (W/cm^2)	3.6–221.7	±2.6–0.4%
T_b (°C)	22–116	±0.1–1
T_{sat} (°C)	25	±0.1
ΔT_{sub} (K)	0	±0.5
p_{in} (kPa)	273	±1.5
Δp (kPa)	0.3–105	±0.65
α (kW/m^2 K)	1.2–26.8	±2–22%
x_{out}	0.02–0.75	±9–0.6%

$$T_{fin}(H) = T_{fl} + \frac{(T_b - T_{fl})}{\cosh(mH) + \frac{\alpha}{m \cdot k_{Si}} \cdot \sinh(mH)} \quad (27)$$

All R236fa properties were calculated with the REFPROP 7.0 software from NIST. The uncertainty analysis was performed with the propagation method proposed by Kline and Mac Clintock [25] and presented in Table 1.

5. Single-phase flow validation tests

The first step to validate the test facility and test section was to perform energy balance tests with a highly sub-cooled refrigerant flow ($\Delta T_{sub} = 18$ K). The heat losses to the surroundings were less than 10% for base heat fluxes greater than 3.6 W/cm^2 and less than 2% for base heat fluxes greater than 8.3 W/cm^2. The heat losses to the ambient are always less than 2 W so that the heat losses are mainly due to the thick copper wire connecting the heater to the power supply.

The second step was to perform single-phase liquid heat transfer coefficient measurements to validate the measurement technique and the data reduction procedure. The fluid enters the test section with a sub-cooling of 18 K at the maximum pressure sustainable by the test facility and, as the mass flow rate is varied, the heat flux is adjusted so that the maximum possible outlet fluid temperature is obtained, i.e., it is ensured that all the RTDs are below the saturation temperature. This method ensured that for each Reynolds number the fluid temperature rise was large enough to have a low uncertainty. The results of these measurements are shown in Fig. 6. The upper graph shows the average of the five Nusselt numbers measured at the location of each RTD versus the average Reynolds number, with the estimated errors in both directions included in the size of the symbol, compared with the numerical solution of Shah and London [22] for a hydrodynamically and

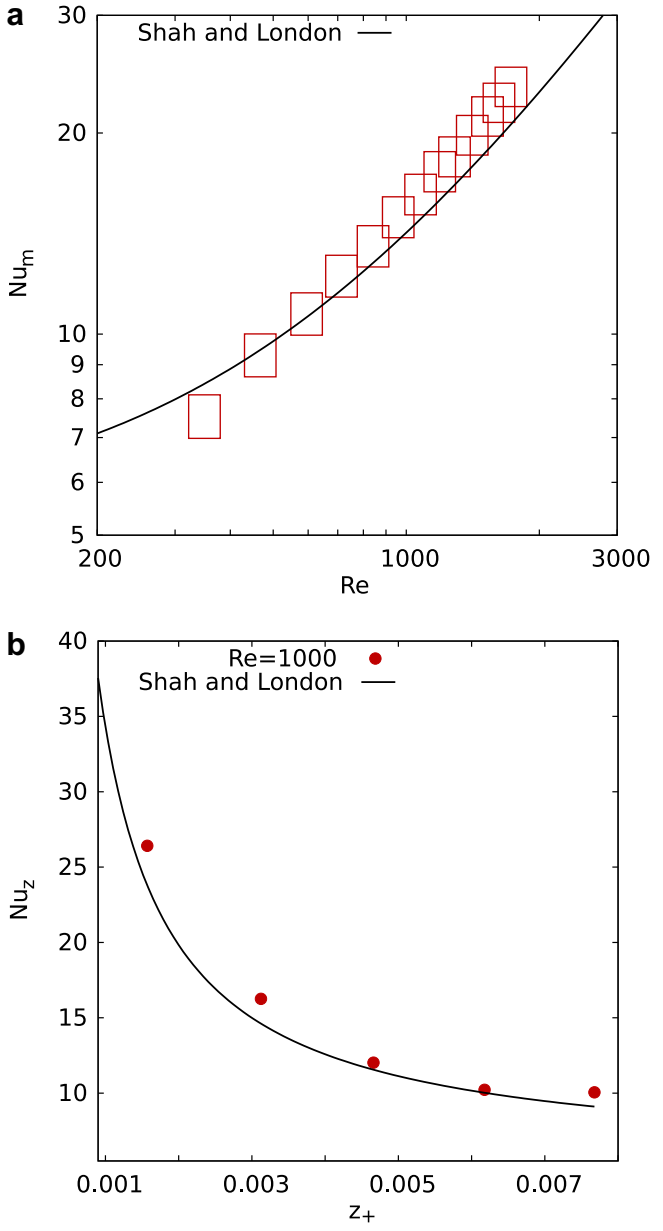

Fig. 6. Liquid Nusselt number. (a): average Nusselt number versus Reynolds number. (b): local Nusselt number versus reduced flow length.

thermally developing laminar flow with three sides subject to a uniform heat flux. The lower graph shows a set of local Nusselt numbers plotted versus the reduced flow length defined by Eq. (4) for a fixed Reynolds number. These experimental Nusselt numbers show a very good agreement with the theoretical solutions and in particular for the development of the boundary layer on the lower graph of Fig. 6. The deviation from the theoretical solution at the lowest Reynolds number (<350) is probably due to axial heat conduction since the heat transfer coefficient is very low in this region and the heat balance is not as good as noted earlier. Nonetheless, the agreement is very good and validates the integrity of the test facility, measurement system and data reduction method.

6. Flow boiling experimental results

Ten mass velocities between 280 and 1500 kg/m^2 s were tested. For each mass velocity, the system pressure was set at 273 kPa and the sub-cooling to 0 K $\pm$ 0.5 K. Boiling was first initiated in adiabatic conditions by increasing the flow rate until the inlet orifices produced bubbles by cavitation. Then the lowest heat flux (3.6 W/cm^2) was applied to maintain boiling and the flow rate was reduced to the desired value. Data were acquired after steady state was reached. Then 100 data sets were recorded and averaged. The standard deviation was used for the uncertainty calculation as advised by Kline and Mac Clintock [25]. Then, the heat flux was increased by steps of 1 V on the power supply until the maximum possible heat flux for that mass velocity was reached (not CHF, however). The heat flux limitation was due to the maximum pressure drop sustainable by the pump. Steady state could be reached in less than 4 minutes between two successive heat fluxes thanks to the controlled pressure in the reservoir and the small thermal mass of the test section.

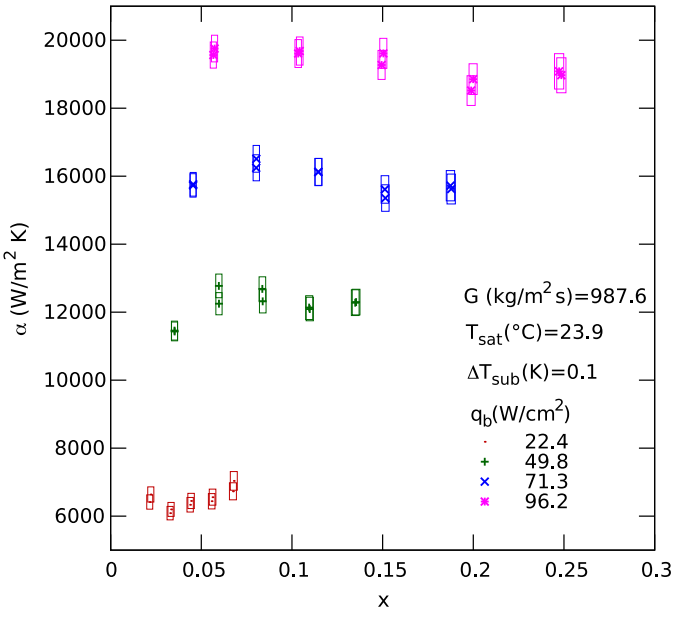

Fig. 7. Reproductibility of the flow boiling heat transfer coefficient measurements.

Fig. 7 shows the results of the reproducibility test for the flow boiling heat transfer measurements. The two sets of data were recorded at a two week interval and the test section and manifold cover had been disassembled and reassembled between the two tests. Furthermore, the inlet pressure drop for the second test was half that for the first test because the size of the inlet slit was increased. As a consequence, it can be concluded that (i) the data are reproducible and (ii) the inlet pressure drop is correctly taken into account in the data reduction procedure.

Figs. 8–12 show the entire local heat transfer database as a function of the local vapour quality for the 10 different mass velocities, with up to 31 base heat flux steps between 3.6 and 221 W/cm^2. These are believed to be the highest heat fluxes used in heat transfer measurements to date for a refrigerant boiling in a microchannel.

Fig. 13a, for fixed vapour qualities between 2% and 8%, shows the heat transfer coefficient as a function of the wall heat flux q_w. The heat transfer coefficients and wall heat fluxes q_w are defined with respect to the effective heat transfer area calculated using the fin efficiency of the fins separating the channels, with Eqs. (20) and (23), respectively. The so-called "boiling curve" yields an exponent of 0.67 at high heat flux and a heat transfer coefficient that is

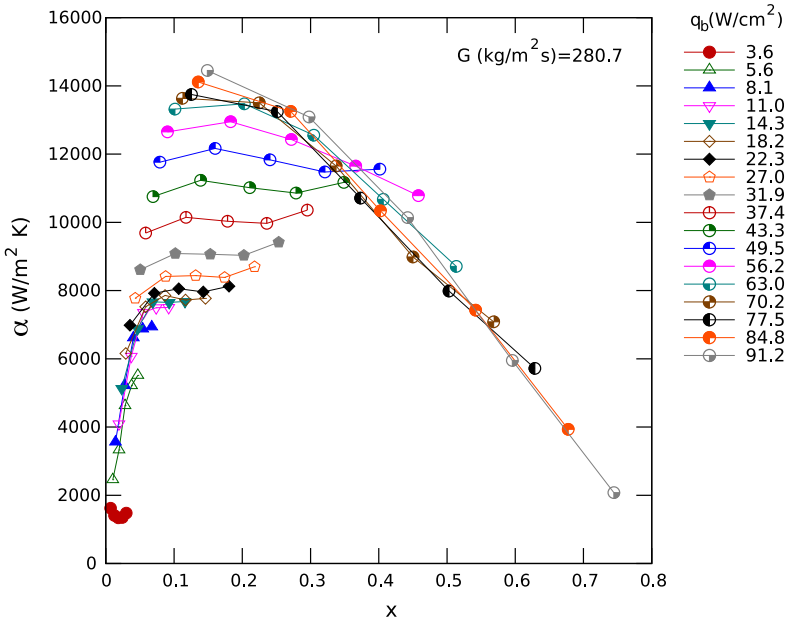

Fig. 8. Local flow boiling heat transfer coefficient versus local vapour quality for increasing base heat fluxes. Mass velocity of 281 kg/m^2 s.

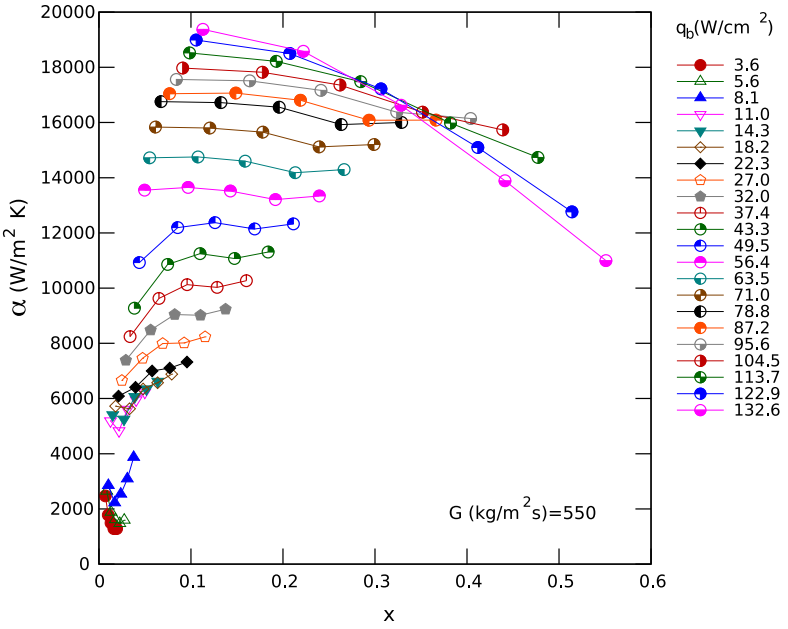

Fig. 9. Local flow boiling heat transfer coefficient versus local vapour quality for increasing base heat fluxes. Mass velocity of 550 kg/m^2 s.

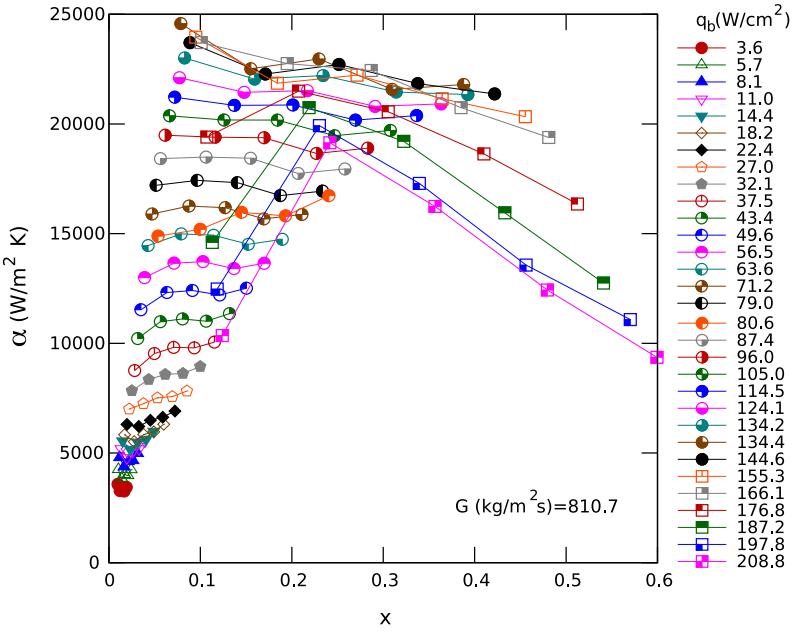

Fig. 10. Local flow boiling heat transfer coefficient versus local vapour quality for increasing base heat fluxes. Mass velocity of 811 kg/m^2 s.

nearly constant or slightly increasing with heat flux at lower heat flux. From an application point of view it is important to know the junction temperature, i.e., where the heater and the thermal paste are in contact. Thus, Fig. 13b shows the local heater base temperature versus local vapour quality for increasing heat fluxes. Finally, Fig. 14 shows the local heat transfer coefficient as a function of the local vapour quality, for various mass velocities between 281 and 1501 kg/m^2 s, for fixed heat fluxes of 37.7 and 103.3 W/cm^2.

Fig. 8 shows the heat transfer coefficient versus vapour quality at mass velocities of 280.7 kg/m^2 s. At low heat flux ($q < 27$ W/cm^2) the heat transfer coefficient increases with vapour quality and increases very little with heat flux. For moderate heat fluxes ($27 \leqslant q \leqslant 49.5$ W/cm^2, the heat transfer coefficient varies little with vapour quality and increases with heat flux. At higher heat fluxes ($q > 49.5$ W/cm^2, the heat transfer coefficient decreases strongly with the vapour quality and decreases slightly with heat flux.

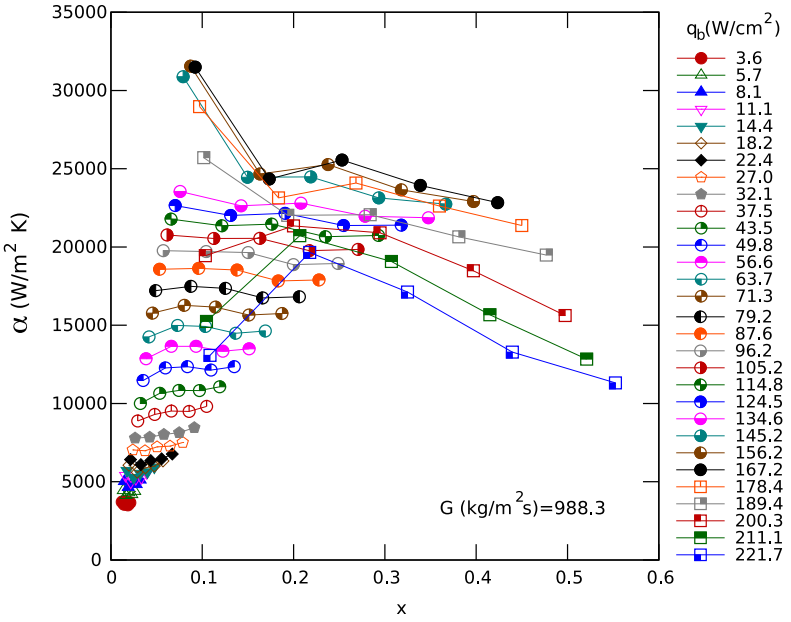

Fig. 11. Local flow boiling heat transfer coefficient versus local vapour quality for increasing base heat fluxes. Mass velocity of 988 kg/m^2 s.

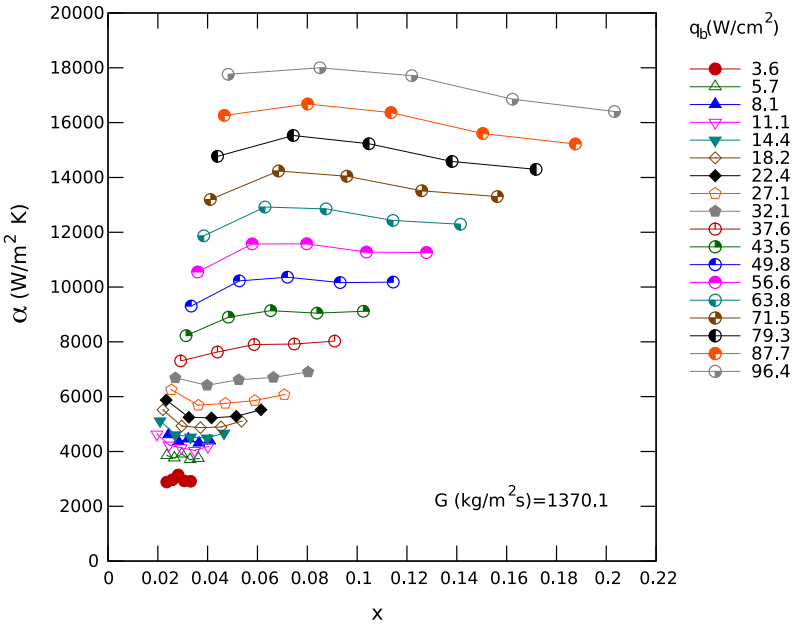

Fig. 12. Local flow boiling heat transfer coefficient versus local vapour quality for increasing base heat fluxes. Mass velocity of 1370 kg/m^2 s.

Fig. 9 shows the heat transfer coefficient versus vapour quality at mass velocities of 550 kg/m^2 s. At low heat flux ($q < 27$ W/cm^2) the heat transfer coefficient increases with vapour quality and increases very little with heat flux. For moderate heat fluxes ($27 \leqslant q \leqslant 95.6$ W/cm^2, the heat transfer coefficient varies little with vapour quality and increases with heat flux. At higher heat fluxes ($q > 95.6$ W/cm^2, the heat transfer coefficient decreases strongly with the vapour quality and decreases with the heat flux.

Figs. 10 and 11 show the heat transfer coefficient versus vapour quality at mass velocities of 810.7 and 988.3 kg/m^2 s. At low heat flux ($q < 27$ W/cm^2) the heat transfer coefficient increases with vapour quality and increases very little with heat flux. For moderate heat fluxes ($27 \leqslant q \leqslant 134.6$ W/cm^2), the heat transfer coefficient varies little with vapour quality and increases with heat flux. At higher heat fluxes, the heat transfer coefficient decreases strongly with the vapour quality and is independent of the heat flux. For $q > 189.4$ at 988.3 kg/m^2 s and 166.1 at 810.7 kg/m^2 s, the heat transfer coefficient versus vapour quality curve presents a maximum around $x = 0.2$, then decreases steeply with vapour quality and heat flux.

Fig. 12 shows the heat transfer coefficient versus vapour quality at mass velocities of 1370.1 kg/m^2 s. At low heat

flux ($q < 27$ W/cm^2) the heat transfer coefficient increases very slightly with vapour quality and increases little with heat flux, although more than in the preceding figures. For higher heat fluxes the heat transfer coefficient varies little with vapour quality and increases with heat flux.

Analysis of all these figures leads to the identification of three characteristic trends:

(i) At very high heat fluxes, the heat transfer coefficient increases with mass velocity and decreases with increasing heat flux (situation reached only in Figs. 8–11). It was found that the transition heat flux at which this behaviour is noticeable is proportional to the mass velocity and occurs when $q_b > 0.14 \cdot G$ W/cm^2 (correlation coefficient of 0.97). Furthermore, two sub-trends can be identified in this region:
   (a) for Bo $< 1.35 \times 10^{-2}$ the heat transfer coefficient decreases monotonically with the vapour quality;
   (b) for Bo $> 1.35 \times 10^{-2}$ and $800 < G < 1100$ kg/m^2 s, a peak in the heat transfer coefficient curve appears at $x \approx 0.2$.

(ii) At medium heat fluxes ($60 < q_b < 0.14 \cdot G$ W/cm^2) the heat transfer coefficient is almost independent of vapour quality and increases with heat flux. Fig. 13a shows that in this region α increases like

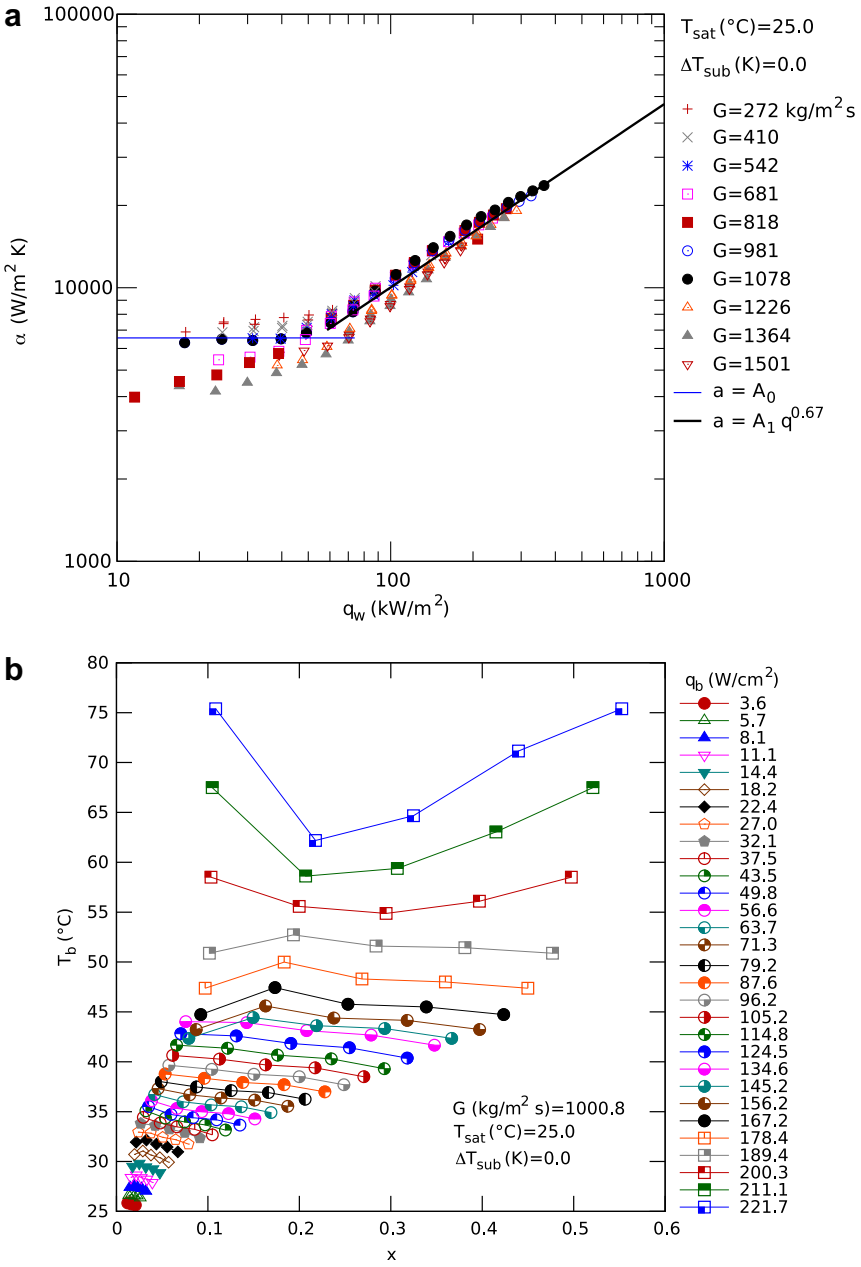

Fig. 13. (a) Flow boiling heat transfer coefficient versus channel wall heat flux at low vapour quality (2–8%). (b) Local base temperature of die versus local vapour quality for increasing base heat fluxes.

$q_w^{0.67}$. Besides, α is independent of G for low and medium G (<1200 kg/m^2 s) and decreases with increasing G at high G (>1200 kg/m^2 s).

(iii) At low vapour quality ($x < 0.1$), low heat flux ($q_b < 60$ W/cm^2 in Fig. 13a) and low to medium mass velocities ($G < 1200$ kg/m^2 s), the heat transfer coefficient increases with vapour quality and is slightly dependent on heat flux and mass velocity.

For trend (i) the peak and subsequent steep decline in the heat transfer coefficient corresponds to the appearance of larger fluctuations in the measured base temperatures and an increase of the heater base temperatures as shown in Fig. 13b. Actually, for trends (ii) and (iii) the statistical fluctuation in the five base temperature measurements is constant with vapour quality, heat flux and mass velocity, approximately equal to 0.02 K. However, at the same time as the heat transfer coefficient starts decreasing quickly with vapour quality, these fluctuations increase up to 0.3 K for the RTD nearest to the exit of the channels but the amplitude of the fluctuations decreases for RTDs closer to the channel inlet. This behaviour is consistent with the occurrence of partial and intermittent dry-out near the exit of the channels, where the vapour quality is higher (but

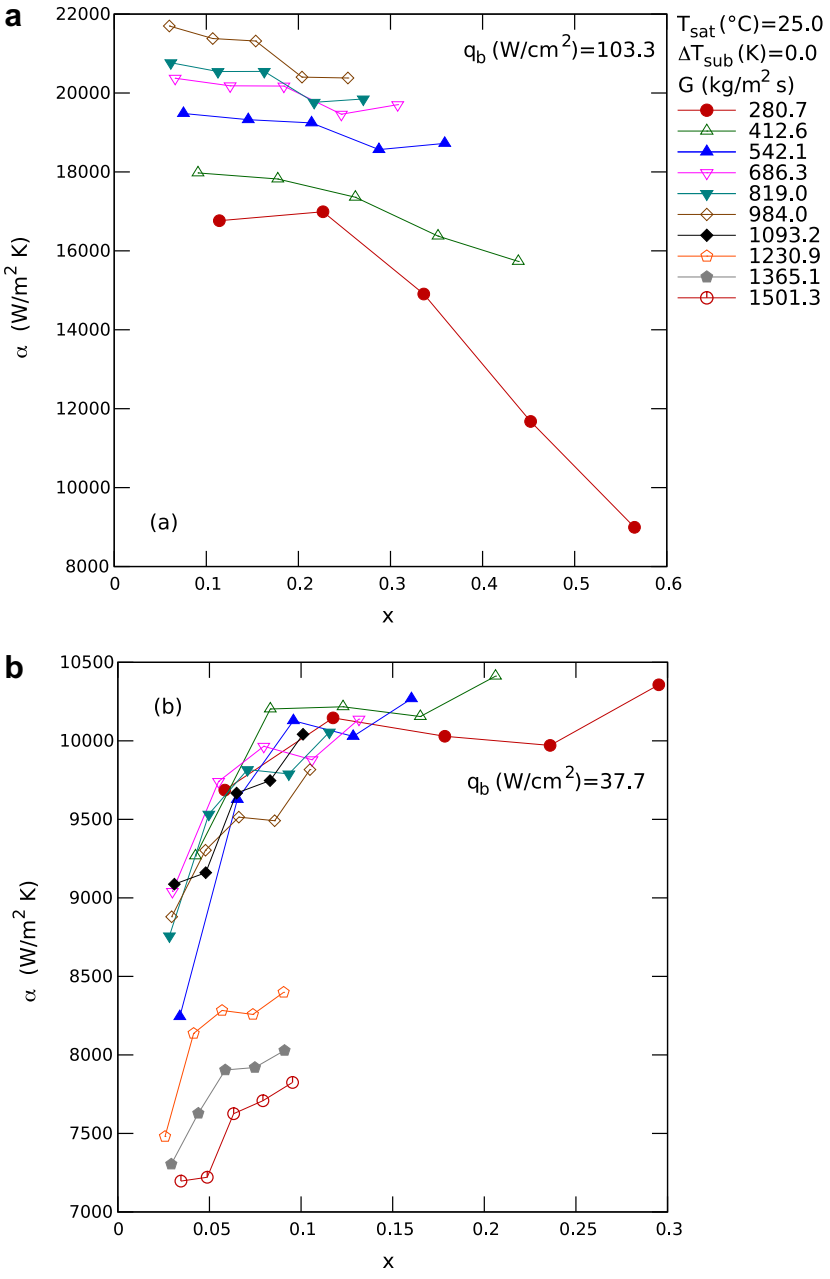

Fig. 14. Flow boiling heat transfer coefficient versus local vapour quality for increasing mass velocities, for base heat fluxes of 37.7 (a) and 103.3 W/cm^2 (b).

should have no influence on the operation of microprocessor chip). This is much smaller than the 30 K fluctuations observed for water by Prasher et al. [26]. Besides, the increase of the heat transfer coefficient with mass velocity is limited, since for a 5.3 times increase in mass velocity the corresponding increase in heat transfer coefficient is only 1.3 at most.

At first glance trend (ii) could be assimilated to nucleate boiling, since the relationship $\alpha \propto q^{0.67}$ is characteristic of nucleate boiling on macrotubes. Actually, an analysis totally different from macroscale models has been presented by Thome et al. [11], who proposed a three-zone model for the elongated bubble flow regime, which is dominant in microchannels. This new model was shown to predict the same heat flux dependence of the heat transfer coefficient as in Fig. 13a with a more realistic heat transfer mechanism. A quantitative comparison of this model with the present data is provided in part II. In this region the heater base temperature is very uniform as shown in Fig. 13b. For example the maximal temperature variation along the channels is only 3 K at 200 W/cm^2 (before the onset of dry-out), which is a big advantage over liquid cooling.

It is not clear why the heat transfer coefficient reaches a maximum and starts to decrease with increasing mass velocity for $G > 1200$ kg/m^2 s. However, this is not very significant since for a 5.3 times increase in mass velocity the corresponding decrease in the heat transfer coefficient is only 30% at most.

The transition from trend (iii) to trend (ii) occurs for a constant base heat flux in the range of 18–22 W/cm^2 whatever the mass velocity. Trend (iii) happens at low heat flux and low vapour quality so that in this region the heat transfer should be strongly dependant on the bubble formation mechanism. Notably, in the present study the bubbles are not generated by a classical wall nucleation process but by cavitation induced by the constrictions at the entrance of each channel. As a consequence, the bubble frequency and therefore the heat transfer coefficient should not depend on the heat flux in this region. If there were no such inlet constrictions this region would correspond to the superheated liquid occurring before classical nucleation starts. At higher heat fluxes, bubbles could also be created by classical wall nucleation, which could explain this transition of the heat transfer trend. Furthermore, one must also consider that the flow enters the channel as a jet through the orifice, impinging on the base of the microchannel before turning and flowing downstream.

7. Conclusions

Local heat transfer coefficients were measured for refrigerant R236fa boiling in a silicon multi-microchannel heat sink for a large range of heat fluxes, mass velocities and vapour qualities. Three main heat transfer trends were outlined. At low heat flux, vapour quality and mass velocity, the heat transfer coefficient increased with vapour quality and was independent of heat flux and mass velocity. At medium heat fluxes the heat transfer coefficient was almost independent of the vapour quality and increased with heat flux. Besides, the heat transfer coefficient was weakly dependant on the mass velocity. At very high heat fluxes the heat transfer coefficient increased weakly with mass velocity and decreased with increasing heat flux. This later trend is probably due to intermittent dry-out before reaching CHF. These results contrast significantly with macroscale flow boiling trends. In particular, the convective boiling regime does not seem to exist in microchannels. The predominance of heat transfer coefficients mainly dependent on heat flux reported by an increasing number of studies is confirmed.

Acknowledgements

The authors wish to thank the Swiss Federal Office for Professional Education and Technology (KTI) for sponsoring this work under Contract No. 6862.2 DCS-NM and for providing the financial support for Dr. Agostini in this project. The authors also wish to recognize the support of the IBM Zürich research center for the construction of the test facility and the fabrication of the test sections.

References

[1] B. Agostini, A. Bontemps, B. Thonon, Effects of geometrical and thermophysical parameters on heat transfer measurements in small diameter channels, Heat Transfer Eng. 27 (1) (2006) 14–24.
[2] P.S. Lee, S.V. Garimella, D. Liu, Investigation of heat transfer in rectangular microchannels, Int. J. Heat Mass Transfer 48 (2005) 1688–1704.
[3] G.P. Celata, M. Cumo, V. Marconi, S.J. McPhail, G. Zummo, Microtube liquid single-phase heat transfer in laminar flow, Int. J. Heat Mass Transfer 49 (2006) 3538–3546.
[4] G.P. Celata, Heat Transfer and Fluid Flow in Microchannels, Begell House, New York, 2004.
[5] S.G. Kandlikar, D. Li, S. Colin, M.R. King, Heat Transfer and Fluid Flow in Minichannels and Microchannels, Elsevier, Amsterdam, 2006.
[6] B. Agostini, M. Fabbri, J.E. Park, L. Wojtan, J.R. Thome, B. Michel, State-of-the-art of high heat flux cooling technologies, Heat Transfer Eng. 28 (4) (2007) 258–281.
[7] B. Agostini, J.R. Thome, Comparison of an extended database of flow boiling heat transfer coefficients in multi-microchannel elements with the three-zone model, in: ECI International Conference on Heat Transfer and Fluid Flow in Microscale, Castelvecchio Pascoli, Italy, 2005.
[8] B. Agostini, A. Bontemps, Vertical flow boiling of refrigerant R134a in small channels, Int. J. Heat Fluid Flow 26 (2005) 296–306.
[9] D. Shiferaw, T. Karayiannis, D.B.R. Kenning, A comparison with the three zone model for flow boiling heat transfer in small diameter tube, in: 13th International Heat Transfer Conference, Sydney, Australia, 2006.
[10] J.R. Thome, Boiling in microchannels: a review of experiment and theory, Int. J. Heat Fluid Flow 25 (2004) 128–139.
[11] J.R. Thome, V. Dupont, A.M. Jacobi, Heat transfer model for evaporation in microchannels. Part I: Presentation of the model, Int. J. Heat Mass Transfer 47 (2004) 3375–3385.
[12] V. Dupont, J.R. Thome, A.M. Jacobi, Heat transfer model for evaporation in microchannels. Part II: Comparison with the database, Int. J. Heat Mass Transfer 47 (2004) 3387–3401.

[13] G. Ribatski, L. Wojtan, J.R. Thome, An analysis of experimental data and prediction methods for two-phase frictional pressure drop and flow boiling heat transfer in micro-scale channels, Exp. Thermal Fluid Sci. 31 (2006) 1–19.
[14] H. Muller-Steinhagen, K. Heck, A simple friction pressure drop correlation for two-phase flow in pipes, Chem. Eng. Process 20 (1986) 297–308.
[15] R. Revellin, V. Dupont, T. Ursenbacher, J.R. Thome, I. Zun, Characterization of diabatic two-phase flows in microchannels: Flow parameter results for R134a in a 0.5 mm channel, Int. J. Multiphase Flow 32 (2006) 755–774.
[16] W.H. McAdams, Vaporization inside horizontal tubes—II—Benzene–oil mixtures, Trans. ASME 64 (1942) 193.
[17] B. Schneider, A. Kosar, Y. Peles, Hydrodynamic cavitation and boiling in refrigerant (R-123) flow inside microchannels, Int. J. Heat Mass Transfer 50 (2007) 2838–2854.
[18] G. Wang, P. Cheng, H. Wu, Unstable and stable flow boiling in parallel microchannels and in a single microchannel, Int. J. Heat Mass Transfer 50 (2007) 4297–4310.
[19] A.E. Bergles, S.G. Kandlikar, On the nature of critical heat flux in microchannels, J. Heat Transfer 127 (2005) 101–107.
[20] J. Lee, I. Mudawar, Two-phase flow in high-heat-flux microchannel heat sink for refrigeration cooling applications: Part II—Heat transfer characteristics, Int. J. Heat Mass Transfer 48 (2005) 941–955.
[21] I.E. Idel'cik, Memento des Pertes de Charge, Eyrolles, Paris, 1979.
[22] R.K. Shah, A.L. London, Laminar Flow Forced Convection in Ducts, Academic Press, New York, 1978.
[23] A. Ciccitti, C. Lombardi, M. Silvestri, G. Soldaini, R. Zavattarelli, Two-phase cooling experiments–pressure drop, heat transfer and burnout measurements, Energ. Nucl. 7 (1960) 407–425.
[24] H.R. Shanks, P.D. Maycock, P.H. Sidles, G.C. Danielson, Thermal conductivity of silicon from 300 to 1400 K, Phys. Rev. 130 (5) (1963) 1743–1748.
[25] S.J. Kline, F.A. McClintock, Describing uncertainties in single-sample experiments, Mech. Eng. 75 (1953) 3–8.
[26] R.S. Prasher, J. Dirner, J.Y. Chang, A. Myers, D. Chau, S. Prstic, D. He, Effect of localized hotspot on the thermal performance of two-phase microchannel heat exchanger, in: Proceedings of ASME InterPACK'05, San Francisco, USA, 2005.